arXiv:2604.06893v4 [cs.CV] 9 Jun 2026

Energy-Regularized Spatial Masking: A Novel Approach to Enhancing Robustness and Interpretability in Vision Models

Tom Devynck[1] , **Djamel Bouchaffra**[1] , **Nadjib Lazaar**[3] , **Mustapha Lebbah**[1]
Bilal Faye[2] , **Hanane Azzag**[2]
[1] DAVID Lab, UVSQ, Paris-Saclay University, Versailles, France
[2] LIPN, UMR CNRS 7030, Sorbonne Paris Nord University, Villetaneuse, France
[3] LISN, Paris-Saclay University, Saclay, France
tom.devynck@uvsq.fr, djamel.bouchaffra@gmail.com,
lazaar@lisn.fr, mustapha.lebbah@uvsq.fr faye@lipn.univ-paris13.fr, azzag@lipn.univ-paris13.fr

Abstract

Deep convolutional neural networks achieve remarkable performance by exhaustively processing dense spatial feature maps, yet this brute-force strategy introduces significant computational redundancy and encourages reliance on spurious background correlations. As a result, modern vision models remain brittle and difficult to interpret. We propose Energy-Regularized Spatial Masking (ERSM), a novel framework that reformulates feature selection as a differentiable energy minimization problem. By embedding a lightweight Energy-Mask Layer inside standard convolutional backbones, each visual token is assigned a scalar energy composed of two competing forces: an intrinsic Unary importance cost and a Pairwise spatial coherence penalty. Unlike prior pruning methods that enforce rigid sparsity budgets or rely on heuristic importance scores, ERSM allows the network to autonomously discover an optimal information-density equilibrium tailored to each input. We validate ERSM on convolutional architectures and demonstrate that it produces emergent sparsity, improved robustness to structured occlusion, and highly interpretable spatial masks, while preserving classification accuracy. Furthermore, we show that the learned energy ranking significantly outperforms magnitude-based pruning in deletion-based robustness tests, revealing ERSM as an intrinsic denoising mechanism that isolates semantic object regions without pixel-level supervision. Code is available at https://github.com/Tom-Dvk/ERSM

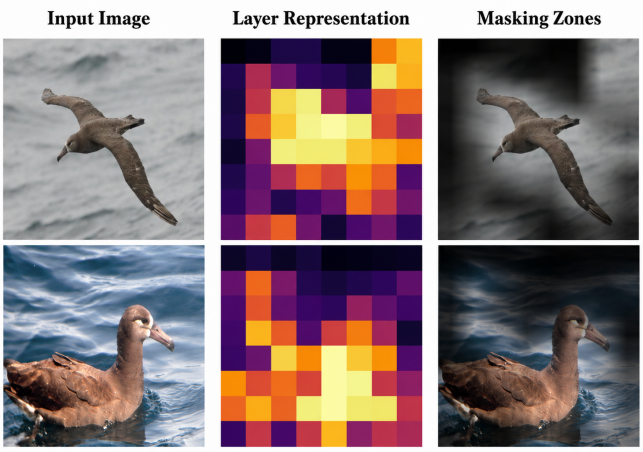

Figure 1: Energy-Based Information Preservation. ERSM adaptively retains semantically relevant features while suppressing background noise.

1 Introduction

The success of deep learning in visual recognition has been driven by dense architectures that process all spatial locations uniformly. While effective, this exhaustive computation introduces significant redundancy and encourages models to rely on spurious background correlations rather than learning semantically meaningful structure. This limitation is especially pronounced in fine-grained classification, where models frequently overfit to contextual cues instead of object-specific features. To address this issue, recent work has explored dynamic inference, enabling input-adaptive computation. Methods such as DynamicViT [Rao *et al.*, 2021], EViT [Liang *et al.*, 2022], and ToMe [Bolya *et al.*, 2023] demonstrate the benefits of adaptivity through token pruning or merging. However, these approaches typically depend on heuristic importance estimates and predefined sparsity schedules, which can discard subtle semantic information in favor of computational efficiency.

Beyond efficiency, interpretability has become a central concern in modern vision systems. Prototype-based models such as ProtoPNet and its deformable extension [Donnelly *et al.*, 2022] provide human-interpretable explanations by matching latent image regions to learned visual prototypes, explicitly modeling geometric variability. However, these methods remain inherently similarity-driven: relevance is inferred from proximity to stored exemplars rather than from an intrinsic principle of information preservation. As a result, they do not directly address a more fundamental question: how much of the visual signal is truly required for correct reasoning?

In contrast, we argue that efficient and interpretable visual representations emerge naturally from a principle of energy minimization. Inspired by statistical mechanics and recent connections between game theory and deep learning [Bouchaffra *et al.*, 2025], we introduce Energy-Regularized Spatial Masking (ERSM), a physics-inspired framework that embeds a differentiable energy system within standard convolutional backbones. Our first contribution is to adapt energy-based modeling from global image generation to internal feature selection, allowing spatial relevance to be inferred from an intrinsic information-preservation principle rather than heuristic importance scores. Second, we model spatial tokens as an interacting system whose forward pass corresponds to an implicit energy-minimization trajectory, eliminating the need for predefined sparsity budgets and enabling input-adaptive computation. Third, we demonstrate that this energy regularization induces emergent, contiguous, and semantically aligned spatial masks that improve robustness and interpretability without segmentation supervision, while remaining lightweight and fully compatible with conventional convolutional architectures.

2 Related Work

A large body of work seeks to reduce spatial redundancy to lower computational costs. DynamicViT [Rao *et al.*, 2021] enforces fixed token keep-rates via a Gumbel-Softmax predictor, EViT [Liang *et al.*, 2022] prunes tokens using class-attention scores, and ToMe [Bolya *et al.*, 2023] further merges similar tokens. While effective for inference speed, these methods treat redundancy purely as a computational concern. In contrast, our ERSM considers redundancy a representational liability: instead of physically removing tensors for wall-clock gains, it masks features to maximize the signal-to-noise ratio. This approach preserves the dense tensor structure of standard CNNs such as ResNet, while conferring the robustness and interpretability benefits typically associated with sparse representations.

Energy-Based Models (EBMs) have regained attention for modeling complex data distributions [LeCun *et al.*, 2006; Grathwohl *et al.*, 2020] and improving out-of-distribution detection. However, conventional EBMs assign energy at the global input level, primarily for generative modeling. In contrast, our ERSM applies EBM principles to internal feature selection, interpreting the forward pass as an energy-minimization trajectory. This perspective bridges generative, physics-inspired principles with discriminative representation learning, enabling the network to selectively preserve semantically relevant features.

While post-hoc methods like Grad-CAM [Selvaraju *et al.*, 2017] visualize importance, they do not influence the model's reasoning. Learnable masking approaches, such as Double-Win Quant [Fu *et al.*, 2021], integrate selection during training but often produce scattered, noisy activation maps due to a lack of spatial constraints. To address this, we draw inspiration from classical computer vision, where Graph-Cut–based energy minimization enforces spatial continuity [Lermé *et al.*, 2010]. Our ERSM adapts this principle to deep feature space: by introducing an explicit pairwise interaction term, we enforce spatial coherence as a core modeling principle, yielding compact, object-aligned masks that are more interpretable than unstructured gating mechanisms.

3 Method

We propose Energy-Regularized Spatial Masking (ERSM), a framework that reformulates feature pruning as a physics-inspired energy minimization problem. Unlike heuristic approaches that impose hard sparsity constraints, ERSM allows the network to autonomously discover an input-adaptive sparsity pattern. We introduce a differentiable Energy-Mask Layer in which retaining a visual token incurs an explicit energy cost. During training, the network balances task performance against the energetic cost of processing redundant spatial features, converging toward an equilibrium that maximizes information density. Notably, ERSM does not seek the exact equilibrium of classical Energy-Based Models, as the energy function does not fully encode all particle interactions; rather, it provides a tractable, discriminative approximation tailored to representation learning.

3.1 Feature Representation

To operationalize the energy formulation, we first discretize the continuous spatial feature map into a set of decision units. Given an intermediate feature map $\mathcal{F} \in \mathbb{R}^{C\times H\times W}$ produced by the convolutional backbone, we apply a spatial unfolding operation that partitions the grid into non-overlapping $d \times d$ patches. This yields a sequence of $N = HW/d^2$ tokens, each encoding the local texture and semantic content of its corresponding region. Let $\mathbf{P} \in \mathbb{R}^{N\times D}$ denote the resulting token matrix, where $D = C \cdot d^2$ is the flattened feature dimension. To stabilize energy computation across varying feature magnitudes, each token $\mathbf{p}_i \in \mathbb{R}^D$ is L_2-normalized, yielding $\hat{\mathbf{p}}_i = \mathbf{p}_i/\|\mathbf{p}_i\|_2$.

3.2 Energy Formulation

We define the energy E_i of a token as the cost of retaining it in the active set. Under the principle of energy minimization, the network is encouraged to suppress tokens with high retention cost. For a feature token $\mathbf{p}_i \in \mathbb{R}^D$, the total energy E_i is defined as:

$$\begin{aligned} E_i =& \lambda_{unary} \times \mathrm{softplus}\underbrace{\left(\mathbf{W}_{\mathrm{mask}}^\top \hat{\mathbf{p}}_i + b_i\right)}_{E_i^{\text{unary}}\text{: Unary Potential}} \\ &+ \lambda_{pair} \times \mathrm{softplus}\underbrace{\left(\sum_{j\in\mathcal{N}(i)} \hat{\mathbf{p}}_i^\top \hat{\mathbf{p}}_j\right)}_{E_i^{\text{pair}}\text{: Pairwise Potential}} \\ &= E_i^{u+} + E_i^{p+} \end{aligned} \tag{1}$$

The first term, E_i^{u+}, corresponds to the unary potential E_i^{Unary}, passed through a $\mathrm{softplus}$ function to enforce positivity and scaled by λ_{unary}. The vector $\mathbf{W}_{\mathrm{mask}} \in \mathbb{R}^D$ is a learned noise template that captures dominant directions of background redundancy rather than object-specific features.

Tokens that align strongly with $\mathbf{W}_{\text{mask}}$ incur a large positive unary energy, increasing their retention cost. In contrast to attention mechanisms that promote aligned features, this alignment penalizes tokens resembling background patterns. Tokens that are semantically distinct (i.e., weakly aligned with the noise template) incur low energy and are therefore inexpensive to retain, allowing informative content to be preserved.

The second term, E_i^{p+}, corresponds to the pairwise potential E_i^{pair}, passed through a $\mathrm{softplus}$ function to enforce positivity and scaled by λ_{pair}. This term explicitly penalizes spatial redundancy, encouraging coherent spatial selection. We define $\mathcal{N}(i)$ as the Moore (8-connected) neighborhood of token i on the token grid. The pairwise term aggregates the cosine similarity between the central token $\mathbf{p}_i$ and its spatial neighbors. In visually homogeneous regions, neighbor similarity is high, yielding a large positive energy penalty and increasing the cost of retaining redundant feature clusters. Minimizing this potential encourages the model to suppress spatially redundant tokens while preserving distinctive, low-cost signals.

Algorithm 1 Energy Mask (Unary and Full Variants)

Require: Feature map $X \in \mathbb{R}^{C\times H\times W}$, patch size D, weights $\lambda_{unary}, \lambda_{pair}$
Ensure: Masked feature map $\tilde{X}$ and diagnostics (m, z, E^{u+}, E^{p+})
$\{\mathbf{p}_i\}_{i=1}^{N} \leftarrow \mathrm{Unfold}(X; D, D)$ *// extract $N = HW/D^2$ spatial patches*
$\hat{\mathbf{p}}_i = \mathbf{p}_i/(\|\mathbf{p}_i\|_2 + \varepsilon) \quad \forall i$ *// patch normalization*
$z_i = \mathbf{w}^\top \hat{\mathbf{p}}_i + b_i \quad \forall i$ *// learned patch importance score*
$m_i \leftarrow \sigma(-z_i) \quad \forall i$ *// soft keep probability*
$E_i^{u+} \leftarrow \lambda_{unary} \cdot \mathrm{softplus}(z_i) \quad \forall i$ *// unary energy cost*
if $\lambda_{pair} > 0$ **then**
  $E_i^{pair} \leftarrow \sum_{j\in\mathcal{N}_8(i)} \langle \hat{\mathbf{p}}_i, \hat{\mathbf{p}}_j\rangle \quad \forall i$ *// local feature coherence: Moore neighborhood (8-connected)*
  $E_i^{p+} \leftarrow \lambda_{pair} \cdot \mathrm{softplus}(E_i^{pair}) \quad \forall i$ *// pairwise energy cost*
else
  $E_i^{p+} \leftarrow 0 \quad \forall i$
end if
$\tilde{\mathbf{p}}_i \leftarrow m_i \cdot \mathbf{p}_i \quad \forall i$ *// soft patch suppression*
$\tilde{X} \leftarrow \mathrm{Fold}(\{\tilde{\mathbf{p}}_i\}; H, W, D, D)$ *// reconstruct masked feature map*
return $\tilde{X}$ and (m, z, E^{u+}, E^{p+})

3.3 Differentiable Gating Policy

To enable end-to-end optimization, we relax the discrete token selection problem into a continuous, differentiable formulation. Unlike standard attention mechanisms that learn to attend based solely on task performance, our framework learns a gating policy guided by energy minimization.

Training Objective: Emergent Sparsity. A key advantage of our approach is that, unlike methods enforcing a fixed sparsity budget ρ (e.g., retaining exactly k patches), we impose a cost on feature retention. The network can retain as many tokens as needed, as long as their contribution to classification performance justifies their energy cost. The regularization loss is defined as the expected energy of the active system. For a batch of N tokens, this corresponds to the mean energy of the retained set:

$$\mathcal{L}_{\text{reg}} = \frac{1}{N}\sum_{i=1}^{N} m_i \cdot E_i \tag{2}$$

where $m_i = \sigma(-E_i^{\text{unary}}) \in [0, 1]$ is the token's continuous retention probability, and E_i its energy cost.

The total training objective combines the task-specific loss with the energy regularization term:

$$\mathcal{L}_{\text{total}} = \mathcal{L}(\mathbf{y}, \hat{\mathbf{y}}) + \mathcal{L}_{\text{reg}} \tag{3}$$

Minimizing this objective leads to an autonomous trade-off: gradient descent drives $m_i \to 1$ (retain) only if the reduction in classification loss $\mathcal{L}$ outweighs the token's energy cost E_i. This produces emergent sparsity, where the number of retained tokens adapts dynamically to the semantic complexity of each input rather than being fixed by a hyperparameter.

Amortized Inference via Implicit Distillation. While the global energy $E_{\text{total}} = \sum_i E_i$ (including pairwise interactions) guides token selection during training, computing it at inference is costly. To address this, we employ amortized inference, where gating decisions rely solely on the local unary potential. Token activation is interpreted as a stochastic equilibrium process. For each token i, the retention decision is driven by the unary penalty:

$$E_i^{\text{unary}} = \mathbf{W}_{\text{mask}}^\top \hat{\mathbf{p}}_i + b_i.$$

where $\mathbf{W}_{\text{mask}}$ serves as a learned redundancy prototype. Tokens aligned with this vector incur high energy and are likely suppressed. The probability of retaining a token is therefore:

$$\sigma(-E_i^{\text{unary}}) = \frac{e^{-E_i^{\text{unary}}}}{1 + e^{-E_i^{\text{unary}}}}.$$

The logic is consistent: low energy implies stability. Tokens that poorly match the noise template (low E_i^{unary}) have $\sigma(-E_i^{\text{unary}}) \to 1$, while high-energy tokens are unstable and likely dropped. Although decisions are local, the weights $\mathbf{W}_{\text{mask}}$ are shaped by the full energy objective during training, effectively distilling global constraints into a fast, local inference policy.

While we refer to $E_{\text{total}} = \sum_i E_i$ as an energy function, it does not define an explicit energy-based probabilistic model; rather, it serves as a training-time regularizer inspired by energy-based principles.

3.4 Gradient Dynamics

Our framework decouples the decision policy from energy evaluation, functioning as a differentiable mechanism embedded within the layer. The forward pass is efficient, producing gating decisions using only the local unary projection $z_i = \mathbf{w}^\top \hat{\mathbf{p}}_i$, while the backward pass evaluates decision quality by incorporating the costly pairwise interactions into the

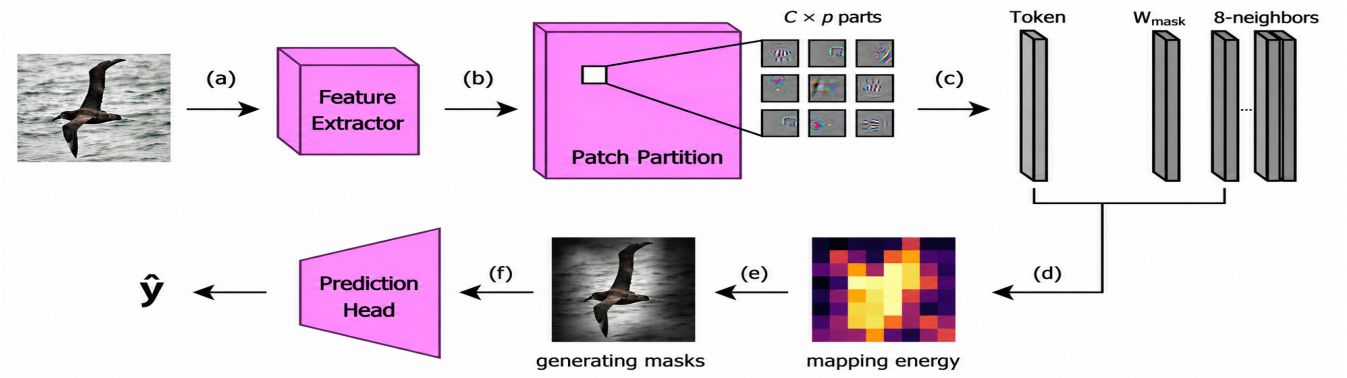

Figure 2: Overview of the Energy-Regularized Spatial Masking (ERSM) framework. (a) A frozen feature extractor encodes the input image. (b–c) The feature map is partitioned into latent tokens. (d) Unary and 8-neighbor pairwise interactions define a token-wise energy. (e) The resulting spatial energy map suppresses redundant background regions. (f) The refined features are passed to the prediction head for classification.

loss. For a token with high spatial redundancy, the pairwise energy E_i^{pair} is large. Minimizing the loss drives the retention mask m_i toward zero.

Mechanically, this negative gradient pressure aligns the weights $\mathbf{w}$ more closely with $\hat{\mathbf{p}}_i$, increasing the noise projection z_i. Over training, the unary filter $\mathbf{w}$ effectively *memorizes* redundant textures, distilling global neighborhood constraints into a local linear projection. This enables future forward passes to suppress redundant features without explicitly computing pairwise interactions.

4 Experiments

We first validate ERSM in a controlled pilot setting before integrating it into standard deep learning backbones. Specifically, we evaluate its behavior and robustness on both shallow CNNs and larger architectures (e.g., ResNet variants [He *et al.*, 2016]), enabling us to isolate its effect independently of backbone depth and capacity. Importantly, these experiments are not intended to push state-of-the-art performance, but to cleanly quantify the contribution of the ERSM layer by comparing otherwise identical models with and without ERSM under controlled conditions.

4.1 Controlled Proof of Concept

In this study, ERSM is implemented as a lightweight *Energy-Mask Layer* inserted after the final convolutional stage of a compact CNN trained on the Food-101 dataset [Bossard *et al.*, 2014]. Input images are resized and center-cropped to 224×224. The backbone produces a feature map of size $C \times H \times W$ ($256 \times 14 \times 14$ in our setting), which is partitioned into non-overlapping $d \times d$ patches ($d = 2$), yielding a 7×7 grid of $N = 49$ tokens. Each token is represented by a vector of dimension $D = C \cdot d^2$.

ERSM computes a per-token unary score $z_i = \mathbf{w}^\top \hat{\mathbf{p}}_i + b_i$ and retains tokens with probability $m_i = \sigma(-z_i)$. Training minimizes the classification loss augmented with the expected energy of retained tokens, $\mathcal{L}_{\text{total}} = \mathcal{L}_{\text{CE}} + \mathcal{L}_{\text{Reg}}$. We perform a two-dimensional sensitivity analysis over the energy coefficients λ_{unary} and λ_{pair} using grid search. For each $(\lambda_{\text{unary}}, \lambda_{\text{pair}})$ pair, the model is trained for 20 epochs on a 20% subset of Food-101, and evaluated in terms of test accuracy and emergent sparsity. The configuration $\lambda_{\text{unary}} = \lambda_{\text{pair}} = 10^{-3}$ consistently yields the best accuracy–sparsity trade-off and is used in all subsequent experiments.

4.2 Results

We compare the following variants: (i) a baseline CNN (four convolutional layers with ReLU and max-pooling) without masking; (ii) ERSM-Unary, using only the unary energy term ($\lambda_{\text{pair}} = 0$); (iii) ERSM-Full, combining unary and pairwise energies ($\lambda_{\text{pair}} > 0$); (iv) DropBlock [Ghiasi *et al.*, 2018]; (v) Spatial Dropout [Tompson *et al.*, 2015]; and (vi) L_0 gating [Louizos *et al.*, 2018], a patch-wise gating baseline with an L_0 sparsity penalty. All models are trained for 100 epochs using AdamW with cosine learning-rate scheduling.

ERSM layer is inserted after the final convolutional block, operating on 14×14 feature maps with 2×2 spatial patches and 256 channels. All models are trained for 100 epochs with identical optimization settings. Table 1 reports the peak test accuracy for each method.

Model	Acc. (%) ↑	$\mathbb{E}[m_i]$
Baseline CNN	69.14 ± 0.22	–
DropBlock	69.53 ± 0.22	–
Spatial Dropout	68.88 ± 0.34	–
L0-Gating	**69.86** ± 0.30	0.65
ERSM-Unary (ours)	69.76 ± **0.15**	0.65
ERSM-Full (ours)	69.73 ± 0.36	0.64

Table 1: Classification performance on Food-101 (Mean ± Std over 5 seeds).

ERSM-Unary achieves performance comparable to the state-of-the-art L0-Gating (69.76% vs 69.86%), while learning a sparse soft gating over spatial patches, with an average keep probability of ≈ 0.65. This indicates consistent suppression of redundant spatial features while maintaining strong

generalization. Notably, ERSM-Unary exhibits lower variance across random initializations than L_0 gating, suggesting more stable and robust convergence under the energy-based formulation.

This structured behavior emerges solely from the optimization objective, without explicit supervision or heuristic saliency mechanisms, highlighting ERSM's ability to discover meaningful spatial organization within convolutional feature maps.

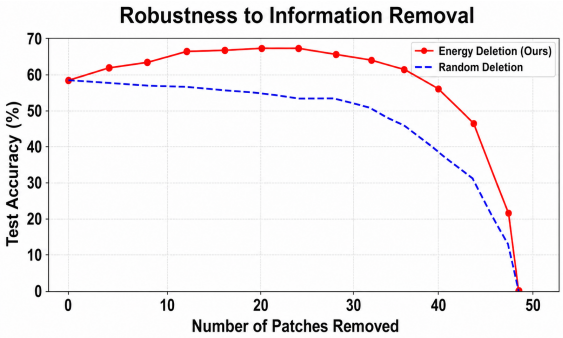

Figure 3: Accuracy under progressive patch removal on the experimental CNN. ERSM preserves more accuracy than random deletion, peaking after removing 20%–25% of patches, highlighting its implicit feature-selection ability.

To assess whether the learned energy scores capture meaningful spatial importance, we conduct a controlled deletion study on the test set. For each input, patches are ranked by their energy scores z_i, and the top-k patches are progressively removed at the feature-map level. After deletion, global average pooling is rescaled by the ratio of total to remaining patches to preserve activation magnitude. This counterfactual evaluation differs from standard inference, which uses soft gating, but enables direct probing of the l earned importance ranking. As a baseline, random deletion is performed by sampling a random permutation of patch indices for each input and removing the first k patches. The same hard suppression and pooling rescaling are applied in both cases, ensuring a fair comparison between energy-based and random deletion.

Figure 3 shows classification accuracy as a function of the number of removed patches. Energy-guided deletion consistently preserves higher accuracy than random deletion across all removal levels. Interestingly, the ERSM curve initially increases, peaking after removing roughly 20%–25% of patches, before gradually declining. This suggests that the model identifies and discards not only redundant but also mildly harmful features, acting as an implicit feature-selection mechanism that improves generalization. ERSM thus learns a structured, semantically meaningful ordering of spatial features rather than relying on brittle or redundant activations.

5 Scaling the Mechanism

Having validated ERSM in a controlled setting, we next examine its scalability and generalization in deep, industry-standard architectures on complex real-world images.

5.1 General Integration Strategy

The core hypothesis of ERSM is that energy minimization provides a general principle for representation selection, independent of the underlying feature extractor. To test this, we evaluate ERSM as a modular, "plug-and-play" gating mechanism that can be inserted into standard convolutional backbones without architectural changes. Although our experiments focus on convolutional backbones to isolate the contribution of ERSM independently of representational capacity, the Energy-Mask Layer is architecture-agnostic. ERSM operates on any sequence of spatial tokens, a condition satisfied by multiple vision paradigms. In Vision Transformers (ViT), tokens correspond directly to image patches, making ERSM integration structurally straightforward: unary and pairwise energies can be computed over patch embeddings prior to or between transformer blocks. This extends naturally to self-supervised variants such as MAE, which expose the same tokenized representation. Likewise, state-space vision architectures (e.g., Vim, VMamba) expose ordered spatial token sequences compatible with ERSM. We therefore view ERSM as a general energy-based token selection principle rather than a CNN-specific mechanism. Scaling from small models to modern backbones introduces two challenges: (1) high-dimensional feature spaces with distributed semantic signals, and (2) maintaining robust energy rankings despite complex texture biases in real-world data. To isolate ERSM's ability to identify intrinsic features independently of backbone capacity, we adopt a frozen-backbone protocol: pretrained weights are fixed up to the insertion point, and only the ERSM parameters and final classifier are trained. This treats the backbone as a fixed semantic sensor and forces ERSM to act as a post-hoc attentional filter operating solely on existing feature correlations.

ERSM is inserted at the final feature layer of the backbone, just before pooling and classification. At this stage, representations encode high-level semantic parts rather than low-level textures, making energy-based ranking more reliable and task-relevant. Late insertion also minimizes computational cost by operating on the smallest feature map. Empirically, earlier insertion produced less stable energy scores and weaker gains, supporting the choice of a late-stage integration.

While the frozen-backbone protocol was deliberately chosen to isolate the effect of the ERSM layer independently of backbone capacity, ERSM remains fully differentiable and naturally compatible with end-to-end optimization. The pairwise energy term can be interpreted as a spatial smoothness prior, penalizing homogeneous redundant activations and encouraging the emergence of locally distinctive feature representations. In this setting, the backbone and ERSM layer would co-adapt during training, potentially yielding sparser and more semantically concentrated representations. We leave systematic investigation of end-to-end training dynamics as future work.

6 Fine-Grained Benchmark Experiments

To evaluate the generality of ERSM across semantic domains, we extend our experiments from generic classification to fine-grained visual recognition (FGVC). FGVC provides a challenging testbed for spatial masking, as correct recognition often relies on subtle, localized cues (e.g., facial patterns, fur texture, or vehicle part details) rather than global shape. We evaluate ERSM on both generic and fine-grained benchmarks. For generic classification, we use Food-101 [Bossard *et al.*, 2014]; for fine-grained tasks include Oxford-IIIT Pet [Parkhi *et al.*, 2012] (37 classes) and CUB-200-2011 [Wah *et al.*, 2011] (200 bird species). ERSM is integrated into multiple ImageNet-pretrained backbones, including ResNet-50 [He *et al.*, 2016], ConvNeXt-Tiny [Liu *et al.*, 2022], and EfficientNetV2-S [Tan and Le, 2021]. For each dataset, we report accuracy, masking, deletion robustness, and qualitative analyses.

Quantitative Results. Table 2 summarizes the performance of ERSM-equipped backbones versus frozen baselines. We report test accuracy and total loss. All backbones are pretrained on ImageNet [Deng *et al.*, 2009] and fine-tuned for 20 epochs under the same settings used in the sensitivity analysis. We also explore the impact of input resolution and different patch sizes, while ensuring consistent tokenization.

				Baseline		**ERSM**	
Dataset	**Backbone**	**Res**	**P**	Acc	Loss	Acc	Loss
CUB-200	ResNet-50	224	1	60.20	0.343	60.59	0.263
	ResNet-50	256	1	59.82	0.374	60.67	0.274
	ResNet-50	256	2	59.82	0.374	60.15	0.238
	ResNet-50	448	1	45.81	0.880	47.67	0.611
	ResNet-50	448	2	45.81	0.880	47.38	0.581
	ConvNeXt-Tiny	224	1	69.83	1.450	69.73	1.415
	ConvNeXt-Tiny	256	2	68.88	1.609	70.62	1.342
	EfficientNetV2-S	448	2	61.63	0.654	63.29	0.730
Food-101	ResNet-50	224	1	68.47	0.910	68.42	0.920
	ConvNeXt-Tiny	224	1	78.23	0.922	78.37	0.925
Oxford Pet	ResNet-50	224	1	91.14	0.098	89.45	0.134
	ConvNeXt-Tiny	256	1	93.32	0.215	93.21	0.967
ImageNet-R	ResNet-50	224	1	38.36	0.036	38.68	0.046

Table 2: Baseline (frozen) vs. ERSM across resolutions (Res) and patch sizes (P). Configurations where P does not divide the feature map are omitted. Peak values shown.

Across all backbones and datasets, ERSM provides competitive performance compared to frozen baselines, particularly on CUB-200 and Food-101 where localized discriminative cues are critical. When no result is reported for a given patch size, this corresponds to cases where the chosen patch dimension does not divide the backbone feature map, preventing valid tokenization. Interestingly, ERSM does not uniformly improve performance across datasets. On Oxford-IIIT Pet, gains are marginal or slightly negative relative to the frozen baseline. We hypothesize that this reflects a reduced background-bias regime: pet images are typically object-centered with limited contextual ambiguity, leaving little opportunity for denoising mechanisms to improve representation quality. In contrast, datasets such as CUB-200 contain stronger contextual variability and localized discriminative cues, conditions under which ERSM consistently provides larger benefits. These observations suggest that ERSM is most effective when spurious correlations constitute a meaningful source of predictive bias.

6.1 Ablation Study

We perform a deeper analysis of ERSM dynamics using ResNet-50 on CUB-200 with input size 256 and patch size 1, isolating the effects of spatial resolution and token granularity on energy minimization. The model is trained for 20 epochs with the dual objective of classification loss and energy regularization, converging stably to a peak test accuracy of 60.67% and loss of 0.2737. Importantly, it autonomously reaches a sparsity equilibrium with an average mask value of 0.60, effectively suppressing roughly 40% of the spatial field while preserving high classification performance.

To verify that discarded features are less informative, we analyze the robustness curve (Figure 4), which plots test accuracy as a function of the number of deleted patches, ranked by learned energy (highest first). This evaluation uses deterministic hard pruning, distinct from the soft gating in training. At each step k, the top-k highest-energy patches are set to zero. To ensure accuracy degradation reflects information loss rather than reduced activation magnitude, we apply dynamic rescaling of the remaining features proportional to the retained token count, preventing the classifier from being biased by simple energy scaling.

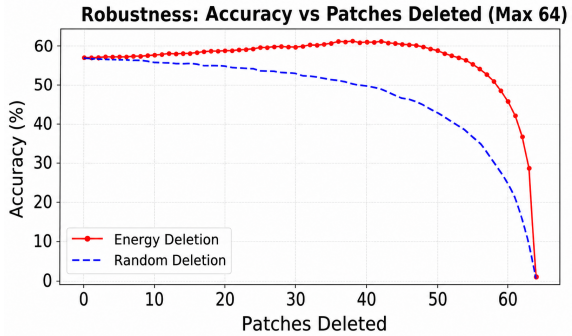

Figure 4: Robustness to Feature Removal on ResNet-50 Res 256 Patch 1. Comparison of classification accuracy under progressive patch deletion using Energy-based ranking (red) versus Random selection (blue).

The resulting robustness profiles in Figure 4 reveal three key phenomena validating the effectiveness of energy-based ranking: **(1)** Unlike the Random Deletion baseline, which shows immediate and monotonic accuracy loss, Energy-Guided Deletion exhibits a convex trajectory. Removing the first 30–40 highest-energy patches actually improves accuracy, indicating that the model assigns high energy to background clutter and spurious correlations. Discarding these distractor patches effectively denoises the representation before any object-relevant features are affected; **(2)** Performance remains well above baseline even after removing up to 50 of the 64 patches. The gap of up to 15 percentage points between energy-guided and random deletion quantifies the strong semantic alignment of the learned energy potential; **(3)**

Accuracy plateaus until a sharp "semantic cliff" occurs after patch 55, where performance collapses. This indicates that the essential discriminative features are concentrated in the final 10–15 lowest-energy tokens, while most of the feature map contributes little or negatively to classification.

6.2 Out-of-Distribution Robustness

To evaluate whether ERSM learns transferable structural information rather than dataset-specific correlations, we perform a preliminary out-of-distribution evaluation using the ResNet-50 configuration (res = 224, p = 1) trained on a 200-class subset of ImageNet and evaluated on ImageNet-R. While top-1 accuracy remains comparable to the frozen baseline, ERSM preserves its characteristic deletion behavior under domain shift: energy-guided patch removal degrades performance substantially more slowly than random deletion, indicating that the learned energy ranking captures structural semantic relevance rather than memorized in-distribution statistics.

6.3 Qualitative analysis

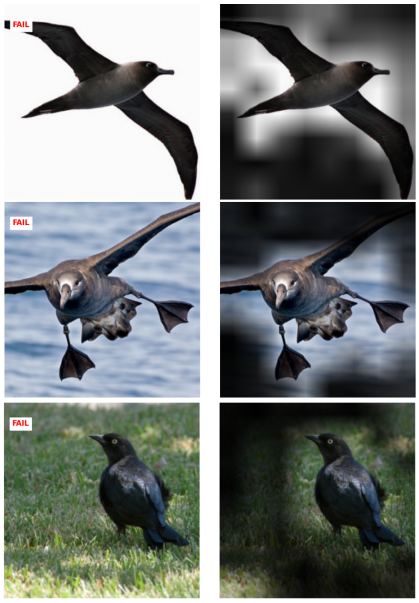

Figure 5: ERSM Improvements. Left: The original image with baseline prediction (Wrong). Right: The ERSM prediction (Correct), showing the learned mask fading out the misleading background.

To understand the decision-making of the ERSM layer, we examine visual examples from inference, categorizing test samples into *Improvements* (where ERSM corrects baseline errors) and *Failure Modes* (where ERSM misclassifies), providing a detailed view of model behavior. Figure 5 shows cases where the frozen ResNet-50 fails but the ERSM-augmented model predicts correctly. These examples often illustrate the "context trap" where the baseline relies on spurious background correlations. ERSM mitigates this by effectively masking misleading context, forcing the classifier to rely solely on intrinsic object features and thereby correcting predictions. Notably, the faded visualizations are not post-hoc saliency maps but direct projections of the model's active decision bottleneck. Token-level keep probabilities $\mathbf{m} \in [0,1]^{H \times W}$ from the ERSM layer are upsampled via bilinear interpolation and applied multiplicatively to the input image. Dark regions correspond to features physically zeroed out in latent space ($m_i \approx 0$), confirming that the classifier made predictions without access to those visual cues.

6.4 Failure Modes of ERSM

We categorize ERSM's failure modes into two types (Figure 6): **(a) Correct masking, misclassification.** The energy mechanism isolates the object and suppresses background, but the classifier fails to distinguish fine-grained traits. This highlights a limitation of the frozen backbone's expressivity rather than the masking policy. **(b) Masking failure.** The model retains substantial background because the energy potential cannot clearly separate object from environment. Such failures often occur in low-contrast images or when background textures resemble the object, confusing the classifier.

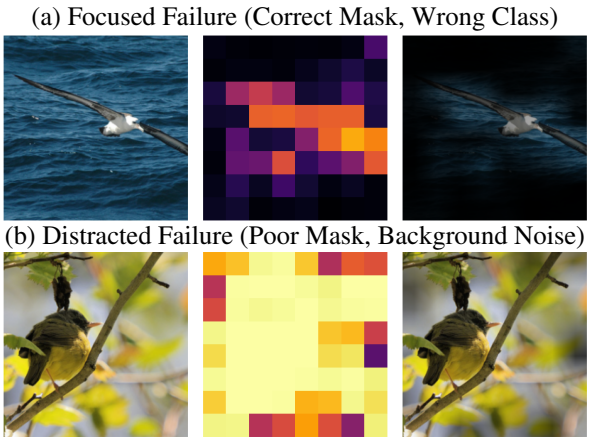

Figure 6: Failure Mode. (a) The model correctly finds the bird but misclassifies it (fine-grained error). (b) The model fails to mask the background, leading to confusion.

7 Conclusion

We introduced Energy-Regularized Spatial Masking (ERSM), a lightweight plug-and-play module that frames spatial feature selection as differentiable energy minimization. By combining unary and pairwise terms, ERSM produces input-adaptive, contiguous masks without segmentation supervision. Experiments show it preserves accuracy while improving interpretability and robustness: energy-guided patch removal outperforms random deletion and can even enhance performance by discarding distracting features. ERSM provides a simple, generalizable framework for energy-based feature selection in vision models.

Acknowledgements

This work has received funding from the European Union Horizon Europe research and innovation programme under the Marie Sklodowska-Curie Actions (MSCA) grant agreement No. 101236749

References

[Bolya *et al.*, 2023] Daniel Bolya, Cheng-Yang Fu, Xiaoliang Dai, Peizhao Zhang, Christoph Feichtenhofer, and Judy Hoffman. Token merging: Your vit but faster. In *International Conference on Learning Representations (ICLR)*, 2023.

[Bossard *et al.*, 2014] Lukas Bossard, Matthieu Guillaumin, and Luc Van Gool. Food-101 – mining discriminative components with random forests. In *Proceedings of the European Conference on Computer Vision (ECCV)*, 2014.

[Bouchaffra *et al.*, 2025] Djamel Bouchaffra, Fayçal Ykhlef, Bilal Faye, Mustapha Lebbah, and Hanene Azzag. Redesigning deep neural networks: Bridging game theory and statistical physics. *Neural Networks*, 191:107807, 2025.

[Deng *et al.*, 2009] Jia Deng, Wei Dong, Richard Socher, Li-Jia Li, Kai Li, and Li Fei-Fei. Imagenet: A large-scale hierarchical image database. In *Proceedings of the IEEE Conference on Computer Vision and Pattern Recognition (CVPR)*, pages 248–255, 2009.

[Donnelly *et al.*, 2022] Jon Donnelly, Alina Jade Barnett, and Chaofan Chen. Deformable protopnet: An interpretable image classifier using deformable prototypes. In *Proceedings of the IEEE/CVF Conference on Computer Vision and Pattern Recognition (CVPR)*, 2022.

[Fu *et al.*, 2021] Yonggan Fu, Qixuan Yu, Meng Li, Vikas Chandra, and Yingyan Lin. Double-win quant: Aggressively winning robustness of quantized deep neural networks via random precision training and inference. In Marina Meila and Tong Zhang, editors, *Proceedings of the 38th International Conference on Machine Learning*, volume 139 of *Proceedings of Machine Learning Research*, pages 3492–3504. PMLR, 18–24 Jul 2021.

[Ghiasi *et al.*, 2018] Golnaz Ghiasi, Tsung-Yi Lin, and Quoc V. Le. Dropblock: A regularization method for convolutional networks. In *Advances in Neural Information Processing Systems (NeurIPS)*, 2018.

[Grathwohl *et al.*, 2020] Will Grathwohl, Kuan-Chieh Wang, Jörn-Henrik Jacobsen, David Duvenaud, Mohammad Norouzi, and Kevin Swersky. Your classifier is secretly an energy based model and you should treat it like one. In *International Conference on Learning Representations (ICLR)*, 2020.

[He *et al.*, 2016] Kaiming He, Xiangyu Zhang, Shaoqing Ren, and Jian Sun. Deep residual learning for image recognition. In *Proceedings of the IEEE Conference on Computer Vision and Pattern Recognition (CVPR)*, 2016.

[LeCun *et al.*, 2006] Yann LeCun, Sumit Chopra, Raia Hadsell, Marc'Aurelio Ranzato, and Fu Jie Huang. A tutorial on energy-based learning. *Predicting Structured Data*, 2006.

[Lermé *et al.*, 2010] Nicolas Lermé, François Malgouyres, and Lucas Létocart. Reducing graphs in graph cut segmentation. In *2010 IEEE International Conference on Image Processing*, pages 3045–3048, 2010.

[Liang *et al.*, 2022] Youwei Liang, Chongjian Ge, Zhan Tong, Yibing Song, Jue Wang, and Pengtao Xie. Not all patches are what you need: Expediting vision transformers via token reorganizations. In *International Conference on Learning Representations (ICLR)*, 2022.

[Liu *et al.*, 2022] Zhuang Liu, Hanzi Mao, Chao-Yuan Wu, Christoph Feichtenhofer, Trevor Darrell, and Saining Xie. A convnet for the 2020s. In *Proceedings of the IEEE/CVF Conference on Computer Vision and Pattern Recognition (CVPR)*, 2022.

[Louizos *et al.*, 2018] Christos Louizos, Max Welling, and Diederik P. Kingma. Learning sparse neural networks through l_0 regularization. In *International Conference on Learning Representations (ICLR)*, 2018.

[Parkhi *et al.*, 2012] Omkar M. Parkhi, Andrea Vedaldi, Andrew Zisserman, and C. V. Jawahar. Cats and dogs. In *Proceedings of the IEEE Conference on Computer Vision and Pattern Recognition (CVPR)*, 2012.

[Rao *et al.*, 2021] Yongming Rao, Wenliang Zhao, Benlin Liu, Jiwen Lu, Jie Zhou, and Cho-Jui Hsieh. Dynamicvit: Efficient vision transformers with dynamic token sparsification. In *Advances in Neural Information Processing Systems (NeurIPS)*, 2021.

[Selvaraju *et al.*, 2017] Ramprasaath R Selvaraju, Michael Cogswell, Abhishek Das, Ramakrishna Vedantam, Devi Parikh, and Dhruv Batra. Grad-cam: Visual explanations from deep networks via gradient-based localization. In *Proceedings of the IEEE International Conference on Computer Vision (ICCV)*, 2017.

[Tan and Le, 2021] Mingxing Tan and Quoc V. Le. Efficientnetv2: Smaller models and faster training. In *Proceedings of the International Conference on Machine Learning (ICML)*, 2021.

[Tompson *et al.*, 2015] Jonathan Tompson, Ross Goroshin, Arjun Jain, Yann LeCun, and Christoph Bregler. Efficient object localization using convolutional networks. In *Proceedings of the IEEE Conference on Computer Vision and Pattern Recognition (CVPR)*, 2015.

[Wah *et al.*, 2011] Catherine Wah, Steve Branson, Peter Welinder, Pietro Perona, and Serge Belongie. The caltech-ucsd birds-200-2011 dataset. Technical report, California Institute of Technology, 2011.